DMSP Space Wx

SSJ, SSIES, SSM Instrument

Data Processing

to

Community Products "User's Guide"

Revision 1.0, January 15, 2015

Artistic representation of a DMSP Block-5D2 spacecraft (source: http://www.af.mil/).

Prepared By: Robert J. Redmon
Contributors: D. Ober, F. Rich, J.V. Rodriguez, D. Knipp, L. Kilcommons

Summary

This is a Public User's Guide. The purpose of this document is to spell out the specifics of the project to create DMSP space weather particles and fields data products in standardized formats that are readily consumable by space weather researchers and their commonly used tools (e.g. CDAWeb). Support has been provided by NOAA/NGDC and NASA grant #NNX13AG07G (PI D. Knipp). This document is a dynamic publicly accessible and authoritative user's guide for the DMSP SSJ, SSIES and SSM data available from the NGDC archive. This User's Guide is a central resource including new information and references to existing documentation offered by AFRL and other contributing institutes (e.g. UTD for SSIES, JHU/APL for SSJ).

This is a fluid, working document. All authors and readers are encouraged to provide comments and criticisms as they arise.

Document Revision History

Date	Description	Preparer	Version
01/15/2015	First version disseminated.	R.J. Redmon	1.0

Table of Contents

1 Introduction

TBD: Add spacecraft image showing instruments and their orientation w.r.t. s/c direction.

Figure 1 illustrates the value of observing a comprehensive set of plasma parameters from the same spaceborne platform, including precipitating electrons and ions, the vector magnetic field, and bulk ion density and vector velocity as measured by the F13 spacecraft during a northern auroral crossing in 1998.

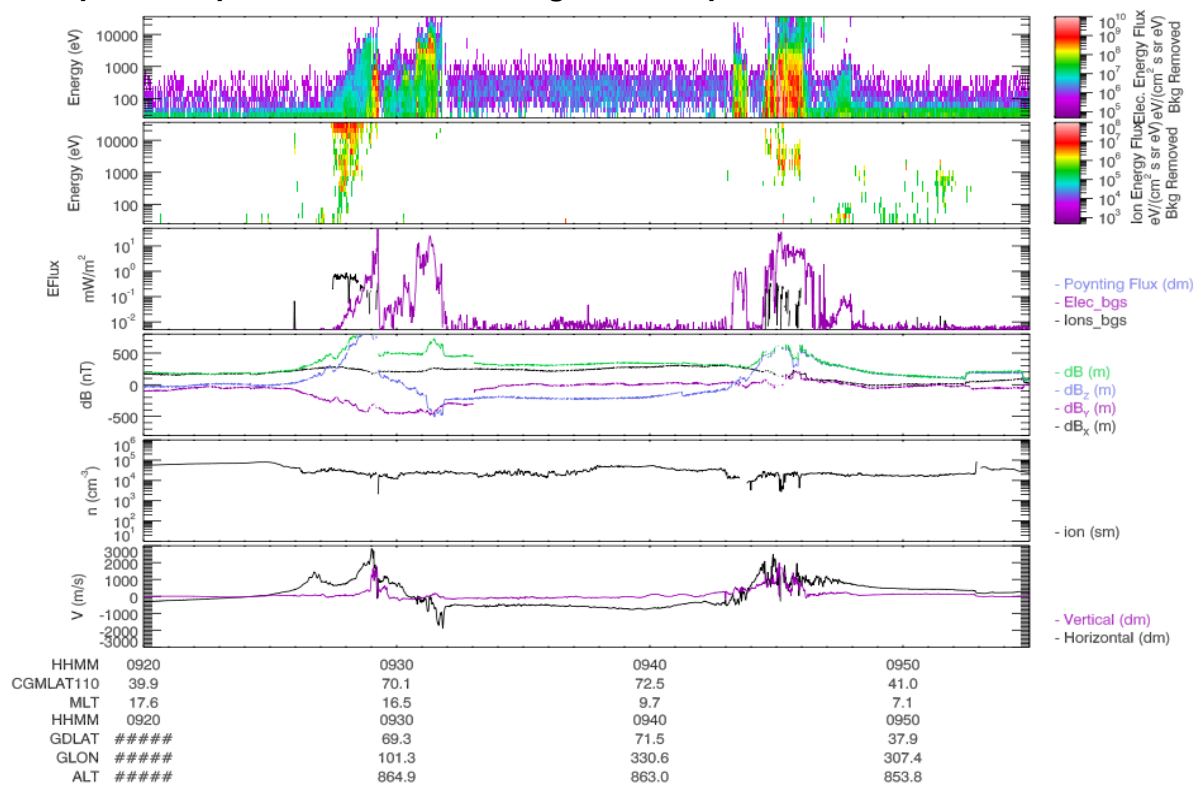**Example stack plot from SSDP showing common parameters for F13 in 1998:**

Figure 1: Time series stack plot using the SSDP application. From top to bottom: a) electron and b) ion differential energy flux (background subtracted) from the SSJ, c) total energy flux for electrons (purple), ions (black) from the SSJ, d) magnetic field deviations from the model given as total (green), and the x- (black), y- (purple) and z- (blue) component directions from the SSM; e) ion density (cm^{-3}) from the Scintillation Meter (SM) , f) bulk velocities from the Ion Drift Meter (IDM) in the spacecraft horizontal (black) and vertical (purple) directions. [TBD: Update x-labels, remove #'s.]

2 Scientific Products, Uncertainties and Quality Flags

Beyond providing quality ephemerides and other contextual information, the final output contains several important scientifically useful products. Alongside these products, known and

propagated uncertainties are also be given.

2.1 Ephemeris

TBD:
- AACGM IDL version used and epoch interpolation
- Backup: Sattrack, SGP4, Celestrak, Kelso, Vallado…
- Correction to doc at Wisconsin eci2geo (and remaining confusion…)

The spacecraft ephemeris is provided in several coordinate frames and on the same cadence and precise timestamps of the measurements (e.g. 1-second for SSJ). The coordinate frames provided are Earth Centered Inertial (ECI) True of Date (TOD) Epoch, Geocentric (GEO), and Altitude Adjusted Corrected Geo Magnetic (AACGM). Here we describe the processing details arriving at these ephemeris coordinate frames. The expected accuracy in the ECI and GEO frames is on the order of a few kilometers.

The DMSP spacecraft estimate their location on board, and telemetry ground processing bundles these 1-minute estimates within instrumental data files which are ultimately conveyed to NGDC via Boston College as day files. These estimated ephemerides are sufficient for operational purposes but are generally in significant disagreement with ephemerides computed in retrospect such as by the North American Aerospace Defense Command (NORAD) and the disagreement should be worse for flight models without on board Global Positioning System (GPS) systems (e.g. F14 and earlier). Interpretation of the vector magnetic measurements is the most sensitive of the environmental measurements to spacecraft location inaccuracies (e.g. Alken et al., 2014; Knipp et al., 2014).

We developed two tools to compute more accurate ephemerides, one based on propagating Two Line Elements (TLE) using the Simplified General Perturbations (SGP) theory (TBD: REF: Vallado et al.; Kelso et al.) and the other based on interpolating $ECI(TOD)$ estimates from the NASA Space Physics Data Facility (SPDF). While, for specific applications, data users may request ephemeris estimates from NGDC using the SGP approach, our standard processing uses the latter approach which we will now describe in greater detail. Two common systems used in practice to specify a coordinate in the ECI frame include the True of Date (TOD) and the "mean equator and equinox of 2000" (J2000) (Tapley et al., 2004, pp. 31, 74). The TOD system identifies the true equator and equinox for the date of the specified coordinate, while the J2000 system is fixed to the date January 1, 2000, 12:00UT. Thus the TOD equinox is time varying in space while the J2000 equinox is fixed. We use the TOD system herein labeled as ECI_{TOD}. We gather 1-minute ECI_{TOD} estimates from the SPDF's Spacecraft Locator tool (http://sscweb.gsfc.nasa.gov/cgi-bin/Locator.cgi), and use an 8th order interpolation (Appendix 7.1) (Burden et al., 1993; Minter 2002) to arrive at the spacecraft location in ECI_{TOD} on the timestamps of environmental measurements. A one day comparison between 1-second ECI_{TOD} and 1-minute ECI_{TOD} interpolated onto the second

(86,400 points) yielded a Root Mean Squared Error (RMSE) less than 6 meters per axis, showing this interpolation scheme to be numerically sufficient.

The IDL Astronomy User's Library (IDLAstro) "eci2geo" routine is then used to rotate our ECI_{TOD} locations to the Geocentric (GEO) frame. The IDLAstro repository and "eci2geo" routine are located at:

        http://idlastro.gsfc.nasa.gov/
        http://idlastro.gsfc.nasa.gov/ftp/pro/astro/eci2geo.pro

Testing of the "eci2geo" routine revealed that it's transformation is most consistent with expecting ECI in the TOD system as it's input and the IDLAstro documentation has been corrected accordingly (private communication P. Saint Hilaire, 2014). We use the Super Dual Auroral Radar Network (SuperDARN) IDL AACGM library (TBD: Ref. R. Barnes; Code Version #; magnetic coefficients through 2010) to transform GEO to AACGM latitude, longitude and Magnetic Local Time (MLT). It's important to ensure various calculators are using the same geocentric radius or to adjust accordingly. IDLAstro "eci2geo" uses a radius of 6378.137 (Earth approximate equatorial radius) while AACGM uses 6371.2 (Earth mean radius). So, we make the minor adjustment before rotating GEO to AACGM. Since AACGM does not use time varying magnetic field coefficients, we approximate the time dependence by linearly interpolating the two AACGM latitude, longitude and MLT estimates computed at the two nearest 5-year epochs onto the instrument timestamp. This is a minor adjustment. Since the latest AACGM magnetic coefficients currently available are from 2010, dates after 2010 are not interpolated.

The ephemeris parameters offered in the public CDF repository are:

Quantity	Units	Description	Dimensionality
SC_ECI	km	Earth Centered Inertial (TOD)	3
SC_GEOCENTRIC_LAT	degrees	Geocentric Latitude	1
SC_GEOCENTRIC_LON	degrees	Geocentric Longitude	1
SC_GEOCENTRIC_R	km	Geocentric Radius	1
SC_AACGM_LAT	degrees	AACGM Latitude	1
SC_AACGM_LON	degrees	AACGM Longitude	1
SC_AACGM_LTIME	hours	AACGM Local Time	1

2.1.1 Ephemeris Validation

TBD.

2.1.2 Caveats and Known Bugs

While we will attempt to minimize bugs, some will show themselves through community usage. They will be prioritized and dealt with as resources permit.

There no known caveats or bugs to document at this time.

2.1.3 Revision History

No revisions to date have been made.

2.2 SSJ Precipitating Electrons and Ions

The SSJ instrument is described in Hardy et al., (1984) and Schumaker et al., (1988) while the theoretical basis for computing particle fluxes from counts is described in Hardy et al., (2008) and herein. The primary output products include original counts, estimated background counts (C), differential energy fluxes (je), integrated energy fluxes (JE), characteristic energy (Eavg), uncertainty estimates (σ) for electrons and ions and the spacecraft ephemeris in multiple frames. The uncertainty measures are estimates and covariances have been assumed to be negligible. Where comparable, the equations for uncertainty developed below are agreeable to Bevington and Robinson (1992). In the section that follows, we describe the calculations from the observed counts to scientifically usable quantities.

The observed count in the i-th channel is compressed onboard then telemetered to the ground and this value is denoted as O_i in this text. The observed counts are also contaminated by penetrating protons and electrons. Since the SSJ instrument lacks a channel dedicated to measuring the penetrating particle flux, processing at NGDC uses a forward-backward variant of the AFRL algorithm to estimate the background. For each observation, we choose the background (B_i) to be the largest of the forward and reverse estimates. The corrected count is given by $C_i = abs(O_i - B_i)$. Note that the adjusted count C_i is forced to be ≥ 0 to be consistent with historical uses and other techniques (e.g. JHU/APL's version of the DMSP adjusted fluxes). A version which allows the adjusted count to float about 0 is available on request. Since original counts (O_i) are provided in the public data set, the end user is free to develop their own background adjustment as they see fit. While O_i is integer valued, B_i and C_i are real valued. Figure 2.1 (TBD) shows original counts and the result from estimating the penetrating particle background to remove proton contamination in the South Atlantic Anomaly and central plasma sheet caused by electron contamination near the sub-auroral horns of the radiation belts.

It is assumed that the counts O_i and B_i are both Poisson distributed and independent. These assumptions are not completely true because: 1) O_i was compressed before telemetering, 2) B_i is estimated from O_i due to a lack of a dedicated background channel, and 3) the adjusted

count C_i is not allowed to be less than 0.

Note that the sum of two independent Poisson random variables is also Poisson (Lehmann, 1986). Considering Poisson counting statistics and telemetry compression the relative 1-sigma uncertainty associated with the measurement of the true count C_i is:

$$\frac{\sigma_{C_i}}{C_i} = \frac{\sqrt{\sigma_{O_i}^2 + \sigma_{B_i}^2 + \sigma_{Compression}^2}}{C_i} ,$$
Equation 2.1

σ_{O_i}, σ_{B_i} : Poisson uncertainties, $\sqrt{O_i}$, and $\sqrt{B_i}$

$\sigma_{Compression(O_i)}$: Telemetry compression, determined numerically (see function ssjdata::get_quantization_uncertainty).

The uncertainty in a count is dominated by Poisson uncertainty (0-100%) and telemetry compression plays only a minor role (0-2%) when the count is less than 3000-4000. Compression dominates the counting error at higher count levels.The interplay is demonstrated in Figure 2.2. Clearly, the relative uncertainty is undefined for a 0 count event, approaching infinity as the count approaches zero, and the standard Poisson distribution is defined for integral mean counts greater than 1. Thus, we set the absolute and relative uncertainties equal to "undefined" (or IEEE NaN) for counts less than 1. Subsequent mathematical operations ignore NaN values.
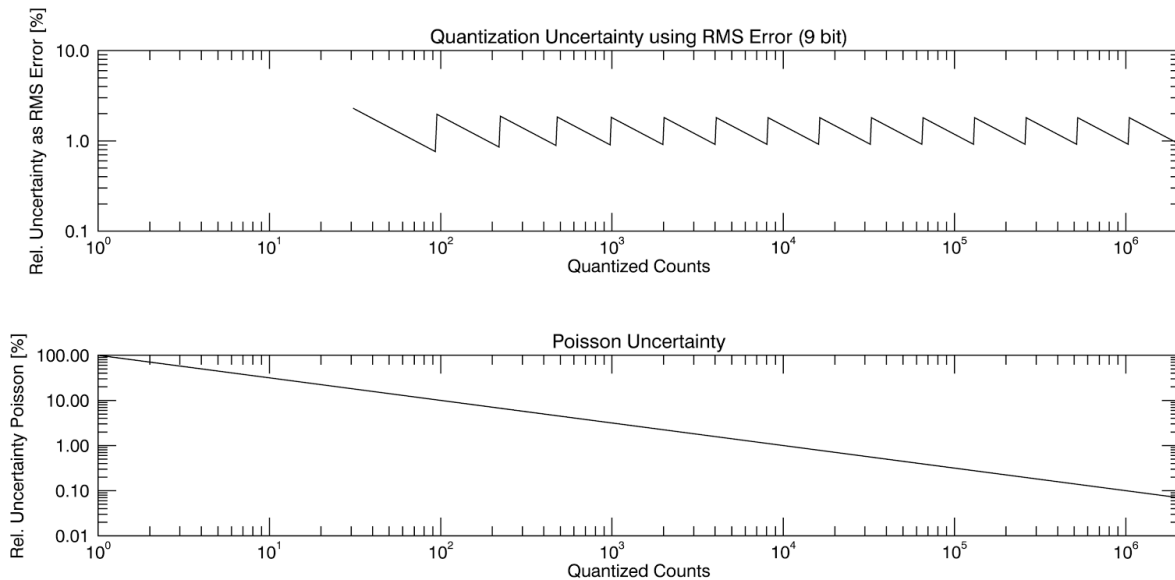

Figure 2.2: Relative uncertainty due to telemetry compression (top) and Poisson counting (bottom) as a function of the count.

Differential electron and ion energy fluxes are calculated from instrument counts. From Hardy et al. (2008) for electrons, we have:

$$j_E(E_i, \Omega) = E j_N(E_i, \Omega) = \frac{C_i \cdot E_i}{\eta_{orbit}(E_i) \cdot \eta_{ground}(E_i) \cdot GF_{ground,i} \cdot \Delta t \cdot \Delta E_i} = \frac{C_i \cdot E_i}{GF_i} \qquad \text{Equation 2.2}$$

$$Units: \ \frac{eV}{cm^2 \cdot s \cdot ster \cdot \Delta eV}$$

where,

i : *channel index, ordered from high to low* ($30 keV$ *down to* $30 eV$)

E_i (eV) : *channel central energy for channel i*

Ω : *angle*

C_i : *counts detected for channel i* (*contaminated by penetrating particles*)

GF_i $(cm^2 sr)$: *effective geometric factor of the sensor* (*see Eq. 2.3*)

$\eta(E_i)$: *efficiency of channel i*

Δt : *dwell time* (*nominally* 0.098 *for up through* $F15$ ($J4$) *and* 0.05 *starting with* $F16$ ($J5$))

ΔE_i : *effective width* (eV) *of channel i* ($FWHM$)

Note that Hardy et al. 2008, uses energy units of keV while we use eV in the current document and the final product files. The channel central energies (E_i) are only nominal. The actual channel response functions can be found in Appendix 7.2 (TBD: get from AFRL).

As noted above, the dwell or integration time per energy is nominally 0.098 seconds for SSJ4 (up through F15) and 0.05 seconds for SSJ5 (F16 and greater). The geometric factors ($GF_{ground,i}$) and channel efficiencies $\eta_{ground}(E_i)$ were determined before launch in the AFRL calibration chamber. As the instrument ages, its degraded efficiency is estimated using methods such as multi-spacecraft intercomparisons and the South Atlantic Anomaly as a standard candle (TBD: ref. Holeman technical memo). Ideally, these four quantities would be separately documented in the final product: $\eta_{orbit}(E_i)$, $\eta_{ground}(E_i)$, $GF_{ground,i}$, Δt and ΔE_i. However, the current version of the product files include the lumped quantity for each of electrons and ions as an effective geometric factor:

$$GF_i = \eta_{orbit}(E_i) \cdot \eta_{ground}(E_i) \cdot GF_{ground,i} \cdot \Delta t \cdot \Delta E_i, \ i \in [1, 19] \qquad \text{Equation 2.3}$$

$$Units: \ cm^2 \cdot ster \cdot sec \cdot \Delta eV$$

Assuming the uncertainty in the differential energy flux $j_E(E_i, \Omega)$ is due predominantly to independent uncertainties in the count (C_i) and the effective geometric factor (GF_i), the uncertainty can be estimated as follows. This assumes that there is no error in the channel energies; in fact, they are uncertain to a few percent.

Given:

σ_{C_i} : *Uncertainty in count, includes Poisson, and telemetry compression* (*see Eq. 2.1*).

σ_{GF_i} : *Uncertainty in effective Geometric Factor. Provided by AFRL.*

Then, the relative uncertainty in the differential number and energy fluxes for channel *i* is:

$$\frac{\sigma_{j_E(E_i,\Omega)}}{j_E(E_i,\Omega)} = \sqrt{\left(\frac{\sigma_{C_i}}{C_i}\right)^2 + \left(\frac{\sigma_{GF_i}}{GF_i}\right)^2} = \frac{\sigma_{j_N(E_i,\Omega)}}{j_N(E_i,\Omega)}$$

<div align="right">*Equation 2.4*</div>

Estimated in this manner, the relative uncertainties in differential energy and number flux are identical. Practically, under significant particle flux, the calibration uncertainty (last quantity in the above equation) dominates the effective uncertainty and this quantity has been estimated by AFRL to be approximately 20% for electrons and 50% for ions (Holeman 2014).

The SSJ4 (up to F15) employs a high energy (949eV - 30keV) and a low energy (30eV - 949eV) detector for each of electrons and ions. Since one of the overlapping 949eV channels is sampled at the beginning of the sample period and the other is sampled at the end, their comparison could be used as a measure of the spatial and temporal variability of the aurora over the scan period (e.g. Hardy et al., TBD:REF). The current version of the processing ignores the highest energy of the low energy detector (~ 949 eV). If we choose at a later date to average the overlapping ~ 949 eV channels (10 and 11) as per:

$$j_E(E_{10,11},\Omega) = \tfrac{1}{2} \cdot (j_E(E_{10},\Omega) + j_E(E_{11},\Omega))$$

<div align="right">*Equation 2.5*</div>

then the resultant uncertainty would become:

$$\frac{\sigma_{jE(E_{10,11},\Omega)}}{j_E(E_{10,11},\Omega)} = \frac{1}{2} \cdot \frac{\sqrt{\sigma_{j_E(E_{10},\Omega)}^2 + \sigma_{j_E(E_{11},\Omega)}^2}}{j_E(E_{10,11},\Omega)}$$

<div align="right">*Equation 2.6*</div>

The total number (energy) flux is calculated in the following manner (adapted from Hardy et al., 2008) by "integrating" differential number (energy) fluxes (Equation 2.2) over energy:

$$J_{N,Total}(\Omega) = j_N(E_1,\Omega) \cdot (E_2 - E_1) + \left[\sum_{i=2}^{18} j_N(E_i,\Omega) \cdot \frac{(E_{i+1} - E_{i-1})}{2}\right] + j_N(E_{19},\Omega) \cdot (E_{19} - E_{18})$$

$$units \ : \ \frac{1}{cm^2 \cdot s \cdot ster}$$

$$J_{E,Total}(\Omega) = j_E(E_1,\Omega) \cdot (E_2 - E_1) + \left[\sum_{i=2}^{18} j_E(E_i,\Omega) \cdot \frac{(E_{i+1} - E_{i-1})}{2}\right] + j_E(E_{19},\Omega) \cdot (E_{19} - E_{18})$$

$$units \ : \ \frac{eV}{cm^2 \cdot s \cdot ster}$$

<div align="right">*Equation 2.7*</div>

The relative uncertainty in the computation of the total number flux $J_{N,Total}(\Omega)$ and total energy flux $J_{E,Total}(\Omega)$ can be estimated as follows assuming channels are uncorrelated (i.e. covariance terms are neglected):

$$\frac{\sigma_{J_{N,Total}(\Omega)}}{J_{N,Total}(\Omega)} \approx \sqrt{\sum_{i=1}^{19} (\Delta E_i \cdot \sigma_{j_N(E_i,\Omega)})^2} \ / \ J_{N,Total}(\Omega)$$

<div align="right">*Equation 2.8*</div>

$$\frac{\sigma_{J_{E,Total}(\Omega)}}{J_{E,Total}(\Omega)} \approx \sqrt{\sum_{i=1}^{19} (\Delta E_i \cdot \sigma_{j_E(E_i,\Omega)})^2} \ / \ J_{E,Total}(\Omega)$$

where,

ΔE_i *are the energy differences* (eV) *in Equation* 2.7

The relationship between the uncertainty in total number and total energy flux is almost trivial (scaled through the channel central energies E_i within the summation).

The characteristic energy is calculated as the ratio of the total energy flux and the total number flux (Hardy et al., 2008):

$$E_{Avg} = \frac{JE_{Total}(\Omega)}{J_{Total}(\Omega)}, \quad units: \ eV \qquad\qquad Equation\ 2.9$$

The relative uncertainty in the computation of the average energy can be estimated as:

$$\frac{\sigma_{E_{Avg}}}{E_{Avg}} \approx \sqrt{\left(\frac{\sigma_{JE_{Total}(\Omega)}}{JE_{Total}(\Omega)}\right)^2 + \left(\frac{\sigma_{J_{Total}(\Omega)}}{J_{Total}(\Omega)}\right)^2 - 2\left(\frac{\sigma(JE_{Total}, J_{Total})}{JE_{Total}(\Omega)\cdot J_{Total}(\Omega)}\right)} \qquad Equation\ 2.10$$

$$\frac{\sigma_{E_{Avg}}}{E_{Avg}} \leq \sqrt{\left(\frac{\sigma_{JE_{Total}(\Omega)}}{JE_{Total}(\Omega)}\right)^2 + \left(\frac{\sigma_{J_{Total}(\Omega)}}{J_{Total}(\Omega)}\right)^2} \qquad \text{(approx. upper bound)}$$

While the uncertainties in the energy and number fluxes are not uncorrelated, for simplicity, we use the first two terms as an upper bound for the uncertainty in E_{Avg}. Numerically, the relative uncertainty in E_{Avg} is roughly 40% greater than that of the relative uncertainty in the integrated energy flux due to the relative variances in the integrated energy and number fluxes being roughly equal.

Figure 2.3 shows an example auroral crossing for F16 2010-01-10, demonstrating the value of computing useful quantities and providing them in a standard format. For the same time range, Figure 2.4 shows the estimated uncertainties in jE, JE, and E_{Avg} for electrons (top) and ions (bottom) clearly demonstrating that the uncertainties are smallest under significant auroral signal and increase significantly outside the auroral zone (owing to low count Poisson uncertainty). In the present version, in the auroral zone, differential flux uncertainties are being thresholded under 100% (Figure 2.4 panels 1 and 4). This issue will be looked at in a subsequent version.
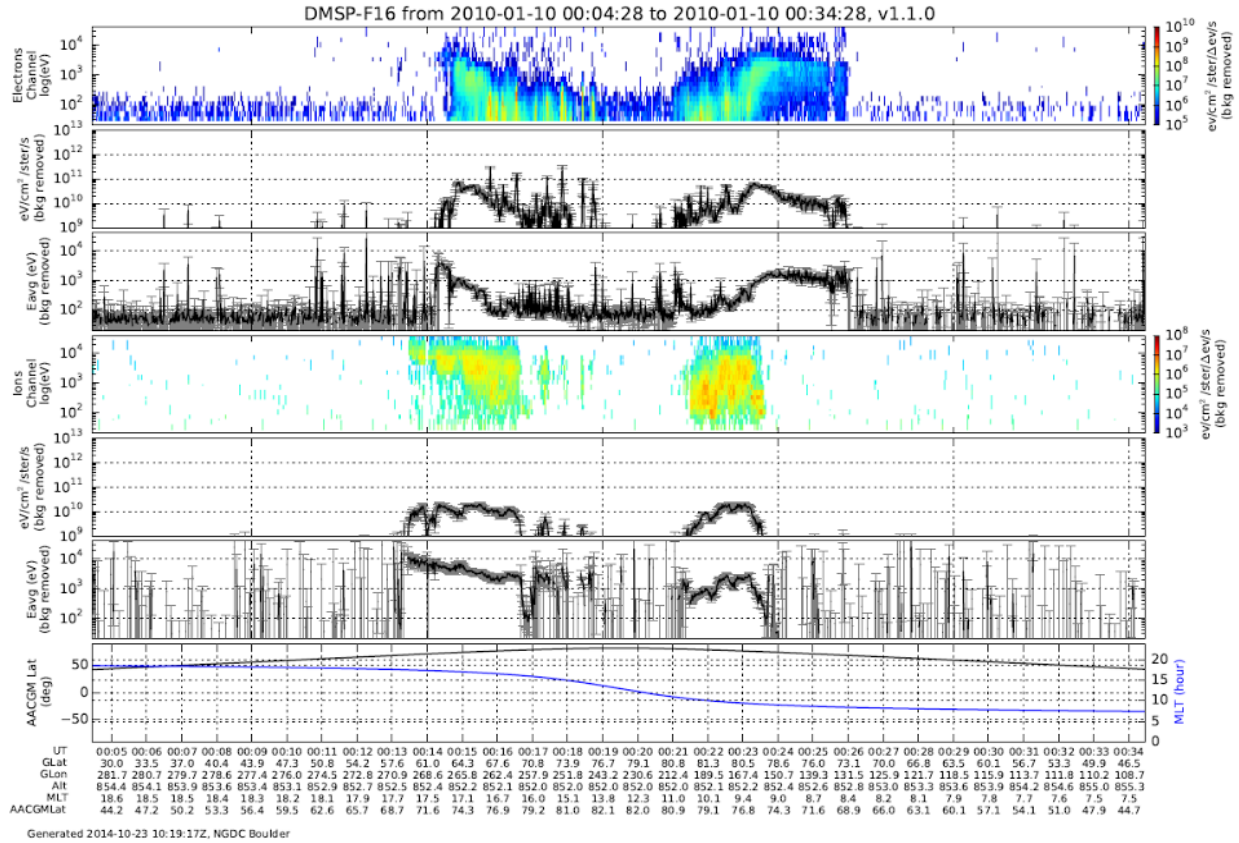
Figure 2.2: F16 2010-01-10 first auroral crossing. Top to bottom: background adjusted electron differential energy flux (jE), integrated energy flux (JE), average energy (E_{avg}); background adjusted ions jE, JE, E_{avg}; AACGM Lat and MLT. Uncertainty bars are shown for the integral quantities but not for the differential quantities.
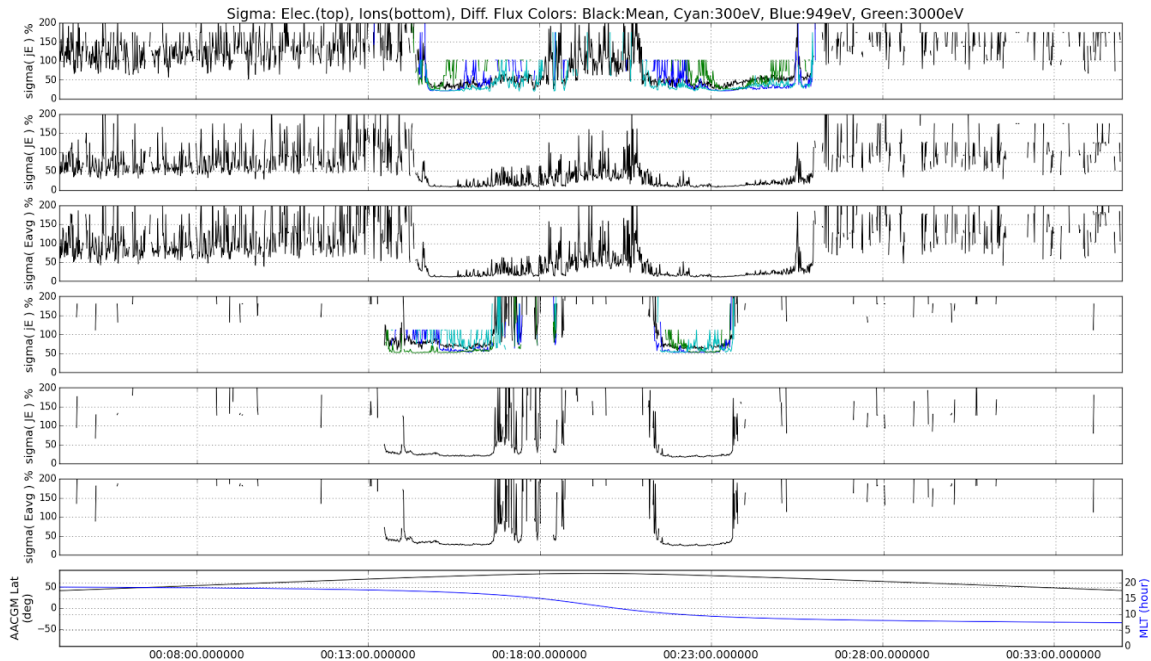
Figure 2.3: Same time range as Figure 2.2. Top to bottom: percent uncertainty in background adjusted electrons JE, E_{Avg}, percent uncertainty in background adjusted ions JE, E_{Avg}, AACGM Lat and MLT. TBD: Since Ci = Oi - Bi, the apparent relative uncertainty thresholding in panels 1 and 4 should be checked.

2.2.1 SSJ Validation

TBD

- Plots comparing SSDP, NGDC, JHU/APL
- Table comparing computations using SSDP, NGDC, JHU/APL

2.2.2 Caveats and Known Bugs

While we will attempt to minimize bugs, some will show themselves through community usage. They will be prioritized and dealt with as resources permit.

TBD: Add notes from B. Emery.

2.2.3 Revision History

TBD.

2.3 SSM Magnetic Field and Perturbations

TBD: Are there any QC flags we can add, perhaps based on (temperature, corrections applied, boom versus body mounted,etc)?

The Special Sensor Magnetometer (SSM) was flown as a body mounted fluxgate vector magnetometer on F12 - F14 and as a boom mounted magnetometer on F15 and later spacecraft. From F. Rich (SSM_Geometry.pdf, 2001), the SSM sensor's right-handed, orthogonal coordinate frame is defined as:
  +x : positive downward along the local vertical direction
  +y : perpendicular to +x in the forward direction of travel
  +z : perpendicular to +x and +y; toward the night side of the orbit plane

Since the spacecraft's velocity vector is not exactly perpendicular to the local vertical direction at all time, there is a very small angle between the SSM +y direction and the spacecraft's velocity vector.

2.3.1 SSM Validation

TBD

2.3.2 Caveats and Known Bugs

While we will attempt to minimize bugs, some will show themselves through community usage. They will be prioritized and dealt with as resources permit.

2.3.3 Revision History

TBD.

2.4 SSIES Bulk Plasma Parameters

TBD: Continue discussions with the folks at UTD along the lines of how to best serve the scientific community for time periods where their DMSP SSIES distribution site provides public data (through 2005).

TBD: Add QC flags (e.g. IDM, RPA).
TBD: Add baseline adjusted perpendicular velocities (nominally Vy, Vz).
TBD: Error bars?

2.4.1 SSIES Validation

TBD.
- Plots and Tables comparing SSDP, NGDC and UTD in 2005 overlap period (from Drew's work).

2.4.2 Caveats and Known Bugs

While we will attempt to minimize bugs, some will show themselves through community usage. They will be prioritized and dealt with as resources permit.

2.4.3 Revision History

TBD.

5 Public Data Access and Tools

Public data access and tools:
- NOAA / NGDC http://satdat.ngdc.noaa.gov/dmsp/
- CDAWeb http://cdaweb.sci.gsfc.nasa.gov/istp_public/
- JHU/APL http://sd-www.jhuapl.edu/Aurora/dataset_list.html
- UTD http://cindispace.utdallas.edu/DMSP/
- Autoplot
- SPEDAS

6 References

TBD: Add:
- DMSP SpWx SSJ SSIES SSM Internal Admin Guide (companion document)
- Coley
- Hardy
- Holeman - in flight SSJ calibration (using the SSA).
- Redmon

- Rich - various tech memos

Bevington, P.R., Robinson, D.K. (1992), Data Reduction And Error Analysis For The Physical Sciences, McGraw-Hill, ISBN 9780079112439.

Burden, R. L. and Faires, J. D., Numerical Analysis, 5th Ed., PWS Publishing Company, Boston, 1993.

Holeman, E. (2014), Geometric Factor Derivation and Calibration Notes, AFRL internal technical memo.

TBD: Kelso REF for celestrak.

Lehmann, E.L. (1986). Testing Statistical Hypotheses (second ed.). New York: Springer Verlag. ISBN 0-387-94919-4. page 65.

Rich, F.J., (2001) Description of DMSP/SSM data for ionospheric/magnetoaspheric research at http://satdat.ngdc.noaa.gov/dmsp/docs/SSM_Geometry.pdf, accessed on January 13, 2014.

Schumaker, T. L. ; Hardy, D. A. ; Moran, S. ; Huber, A. ; McGarity, J. (1988), Precipitating Ion and Electron Detectors (SSJ/4) for the Block 5D/Flight 8 DMSP (Defense Meteorological Satellite Program) Satellite, Air Force Geophysics Lab Hanscom AFB, AFGL-TR-88-0030, Accession Number: ADA203999, 61 pp., http://www.dtic.mil/get-tr-doc/pdf?AD=ADA203999.

TBD: Vallado REF from Space Weather paper.

7 Appendices

7.1 Ephemeris

TBD: add ECI 1-minute to 1-second interpolation information.

7.2 SSJ Detector Efficiencies

TBD, get from AFRL.

7.3 Acronyms

TBD: alphabetize these.

Acronym	Expansion

AACGM	Altitude Adjusted Corrected Geo Magnetic
IDL	Interactive Data Language
ECI	Earth Centered Inertial
J2000	Mean equator and equinox of 2000.0
TOD	True of Date: True equator and equinox
SPDF	Space Physics Data Facility
AFRL	Air Force Research Laboratory
NGDC	National Geophysical Data Center
JHU/APL	Johns Hopkins University Applied Physics Laboratory
CDAWeb	Coordinated Data Analysis Web
SSJ	Special Sensor J
SSM	Special Sensor Magnetometer
SSIES	Special Sensor Ions Electrons and Scintillation
DMSP	Defense Meteorological Satellite Program
UTD	University of Texas Dallas
MLT	Magnetic Local Time